Longitudinal Study of Irradiation-Induced Brain Microstructural Alterations With S-Index, a Diffusion MRI Biomarker, and MR Spectroscopy

Elodie Anne Pérès, Olivier Etienne, Antoine Grigis, Fawzi Boumezbeur, François Dominique Boussin, Denis Le Bihan

International Journal of Radiation Oncology biology • physics

www.redjournal.org

Imaging Radiation Sequelae

Longitudinal Study of Irradiation-Induced Brain Microstructural Alterations With S-Index, a Diffusion MRI Biomarker, and MR Spectroscopy

Elodie Anne Pérès, PhD,*,† Olivier Etienne, MSc,† Antoine Grigis, PhD,* Fawzi Boumezbeur, PhD,* François Dominique Boussin, PhD,† and Denis Le Bihan, MD, PhD*

**NeuroSpin, Frédéric Joliot Institute, Division of Fondamental Research, French Alternative Energy and Atomic Energy Commission, Université Paris-Saclay, Gif-sur-Yvette, France; and †Laboratoire de Radiopathologie, UMR967, Institute of Cellular and Molecular Radiobiology, François Jacob Institute, Division of Fondamental Research, French Alternative Energy and Atomic Energy Commission, French National Institute of Health and Medical Research, Universités Paris-Saclay and Paris-Diderot, Fontenay-aux-Roses, France*

Received Jun 14, 2017, and in revised form Dec 19, 2017. Accepted for publication Jan 22, 2018.

Summary

Cancer patients frequently have cognitive impairments following brain radiation therapy. To monitor irradiation-induced microstructural tissue damage, especially in neurogenic areas, we have investigated the potential of diffusion magnetic resonance imaging and magnetic resonance spectroscopy. The diffusion

Purpose: Radiation therapy is widely used for the treatment of brain tumors, but it may lead to severe cognitive impairments. Previous studies have shown that ionizing irradiation induces demyelination, blood-brain barrier alterations, and impaired neurogenesis in animal models. Hence, noninvasive and sensitive biomarkers of irradiation injury are needed to investigate these effects in patients and improve radiation therapy protocols.

Methods and Materials: The heads of 3-month-old male C57BL/6RJ mice (15 control mice and 15 irradiated mice) were exposed to radiation doses of 3 fractions of 5 Gy from a ^{60}Co source with a medical irradiator. A longitudinal study was performed to investigate cranial irradiation-induced (3 fractions of 5 Gy) microstructural tissue alterations using water diffusion magnetic resonance imaging and magnetic resonance spectroscopy in different areas of the mouse brain (cortex, thalamus, striatum, olfactory bulbs [OBs], hippocampus, and subventricular zone [SVZ]). In addition to the quantification of standard non-Gaussian diffusion parameters, apparent diffusion

Reprint requests to: Denis Le Bihan, MD, PhD, NeuroSpin, CEA Saclay Center, Bat 145, 91191 Gif-sur-Yvette Cedex, France. Tel: +33 (0) 1 69 08 82 05; E-mail: denis.lebihan@gmail.com and François Boussin, PhD, Laboratoire de Radiopathologie, UMR967, Institut de Radiobiologie Cellulaire et Moléculaire, French Alternative Energy and Atomic Energy Commission-French National Institute of Health and Medical Research, 18 route du Panorama, 92260 Fontenay-aux-Roses, France. Tel: +33 (0)1 46 54 97 91; E-mail: boussin@cea.frare

E.P. was responsible for the statistical analysis.

This work was supported by the Life Sciences Division of the Commissariat à l'Energie Atomique et aux Energies Alternatives and Electricité de France. This work was performed on a platform of the France Life Imaging network partly funded by grant ANR-11-INBS-0006.

Conflict of interest: none.

Supplementary material for this article can be found at https://doi.org/10.1016/j.ijrobp.2018.01.070.

Acknowledgments—The authors thank Jean-Baptiste Lahaye for irradiation procedures; Boucif Djemai, Erwan Selingue, and Wilfried Pianezzola for their technical assistance; and Françoise Geffroy for her advice about immunohistology; as well as Cyril Poupon and Luisa Ciobanu for sharing some of their expertise on diffusion- and perfusion-weighted imaging.

Int J Radiation Oncol Biol Phys, Vol. 102, No. 4, pp. 1244–1254, 2018

https://doi.org/10.1016/j.ijrobp.2018.01.070

S-index calculated from the diffusion magnetic resonance imaging signal acquired at 2 optimized values of diffusion weighting appeared as the most sensitive biomarker, revealing subtle brain tissue alterations induced by ionizing irradiation.

coefficient (ADC_0) and kurtosis (K), we evaluated a new composite diffusion metric, designated the S-index (ie, "signature index").

Results: We observed a significant decrease in the S-index in the SVZ from 1 month to 8 months after brain irradiation ($P < .05$). An interesting finding was that, along with a decrease in taurine levels (up to −15% at 2 months, $P < .01$), a delayed S-index drop was observed in the OBs from 4 months after irradiation and maintained until the end of our experiment ($P < .0001$). These observations suggest that S-index variations revealed the irradiation-induced decline of neurogenesis that was further confirmed by a decrease in neural stem cells in the SVZ and in newborn neurons in the OBs of irradiated animals.

Conclusions: This study demonstrates that diffusion magnetic resonance imaging, especially through the S-index approach, is a relevant imaging modality to monitor brain irradiation injury and probe microstructural changes underlying irradiation-induced cognitive deficits.

Introduction

Radiation therapy (RT) is a common treatment of primary brain tumors and metastases, but it may cause severe cognitive impairments affecting the patient's quality of life. Cognitive deficits have been reported in adult brain tumor survivors (who survived >6 months) with an incidence rate of 50% to 90% after partial- or whole-brain irradiation (1-3). The cognitive impairments induced by RT are marked by reduced verbal memory, spatial memory, attention, and novel problem-solving abilities (4-6). Clinically, irradiation-induced brain injury is classified as acute (days to weeks), early delayed (1-6 months), and late delayed (>6 months) (7). The brain injury is characterized by long-lasting vascular abnormalities, demyelination, and, ultimately, white matter necrosis (8-12). Several preclinical studies have shown that irradiation-induced memory and attention deficits are related to neuroinflammation, blood-brain barrier alterations, and demyelination, as well as neurogenesis decline (13-21).

Neurogenesis—the formation of functional, mature neurons from neural stem cells (NSCs) and progenitors—persists throughout life in discrete regions of the adult brain, such as the subgranular zone (SGZ) of the hippocampal dentate gyrus and the subventricular zone (SVZ) lining the lateral ventricles (22). The hippocampus is involved in cognitive processes such as declarative memory and spatial information processing (23), which can be affected by RT and may play a role in irradiation-induced cognitive deficits. Decreased hippocampal neurogenesis and hippocampus-dependent memory dysfunction were reported in adult mice 3 months after cranial irradiation (24, 25). Similarly, whole-brain irradiation decreased the numbers of NSCs and progenitor cells from the SVZ, up to several months after treatment, in a dose-dependent manner (17, 26). Focal irradiation (3 fractions of 5 Gy) of the SVZ induced a long-term neurogenesis decline, leading to a decrease in integration of newborn neurons in the olfactory bulbs (OBs), which ultimately resulted in significant alteration of the olfactory memory in mice (15). Noninvasive and sensitive biomarkers of irradiation-induced injury are still needed to monitor brain damage.

Diffusion magnetic resonance imaging (dMRI) probes tissue at a microscopic scale, well below image resolution, by assessing the random motion of water molecules and their interaction with cell membranes and the cytoskeleton. Consequently, dMRI reveals useful information about tissue microarchitecture (27). Diffusion magnetic resonance imaging (MRI) and its variant, diffusion tensor imaging, which have been widely used in medicine, allow white matter injury in both pediatric and adult patients treated with whole-brain irradiation to be assessed at an early stage (28, 29).

In addition to dMRI, magnetic resonance spectroscopy (MRS) can be used to monitor metabolic alterations induced by irradiation. MRS is a noninvasive technique that can detect and quantify up to 20 brain metabolites (30). In previous studies, MRS has been successfully applied to differentiate irradiation necrosis from brain tumor progression (31, 32), as well as to define an indicator of neurotoxicity induced by brain irradiation (33, 34).

Contrary to most previous preclinical studies using diffusion tensor imaging (35-39) or MRS (40-43), which have focused on investigating early brain injuries in white matter after whole-brain irradiation, our study aimed to establish the time course of structural and metabolic changes occurring in the mouse brain and especially in neurogenesis areas from 3 days to 8 months after whole-brain irradiation. Besides the estimation of non-Gaussian diffusion parameters (apparent diffusion coefficient [ADC_0] and kurtosis parameters) from diffusion-weighted MRI (dMRI) (44), the sensitivity of a novel diffusion metric, designated the S-index, was evaluated. The S-index stands for "signature index" and is a relative distance marker designed directly to identify tissue types (eg, healthy or injured brain) or changes in tissue microstructure. This distance is calculated between the dMRI signal profiles acquired at key b values (chosen to account for both Gaussian and non-Gaussian diffusion properties) using a library of generic signal profiles (signatures) for both tissue types considered (45).

Methods and Materials

Animals

In vivo experiments were performed on 3-month-old C57BL/6 male mice (Janvier, Le Genest-Saint-Isle, France). Animals were maintained with access to food and water ad libitum at a constant temperature (19°C-22°C) and humidity (40%-50%) on a 12-hour light−12-hour dark cycle. Experiments were approved by the regional ethics committee and were performed in accordance with the European Communities Council Directive of September 22, 2010 (EC/2010/63).

Irradiation

Fifteen adult mice were irradiated with an Alcyon medical irradiator (gamma rays, ^{60}Co) as previously described (15, 17). In brief, they were anesthetized with ketamine (Imalgen, 75 mg/kg; Merial, Lyon, France) and medetomidine (Domitor, 1 mg/kg; Pfizer, Paris, France) by the intraperitoneal route. Whole-brain irradiation was achieved using a 10-cm-thick lead shield, with a 12-mm-diameter circular hole positioned right above the mouse's head, protecting the rest of the body. A total dose of 15 Gy was delivered at a dose rate of 1 Gy/min in 3 equal fractions of 5 Gy that were separated by 48-hour intervals. This irradiation protocol to the head alone is not lethal for the mouse and does not induce an irradiation burn to the skin or epilation; only depigmentation of the hair of the head is observed from 4 months after irradiation. After exposure, the mice were woken up via an intraperitoneal injection of atipamezole (Antisedan, 1 mg/kg; Pfizer). The mice were followed longitudinally for up to 8 months using MRI. To ensure that our measures were not reflecting normal brain aging, a control group of nonirradiated animals (15 control mice) was studied in parallel to our irradiated mice.

Magnetic resonance acquisitions

Acquisitions were performed on an 11.7-T MRI scanner equipped with a CryoProbe dedicated for mouse brain imaging (Biospec; Bruker BioSpin, Rheinstetten, Germany). After acquisition of an anatomic T2-weighted MRI scan (Turbo Spin-Echo sequence, echo time [TE], 30 ms; repetition time [TR], 2500 ms; turbo factor, 8; resolution, 50 × 50 × 450 μm), diffusion-weighted images were acquired with the following parameters: Pulsed Gradient Spin-Echo-Echo-Planar Imaging (EPI) sequence; TE, 24 ms; TR, 2500 ms; resolution, 125 × 125 × 450 μm; δ, 4 ms; Δ, 11.5 ms; and 34 b values from 10 to 3500 s/mm^2 (10, 20, 30, 40, 50, 60, 70, 80, 90, 100, 110, 120, 130, 140, 150, 160, 170, 180, 190, 200, 250, 500, 750, 1000, 1250, 1500, 1750, 2000, 2250, 2500, 2750, 3000, 3250, and 3500 s/mm^2). To mitigate gradient hardware asymmetries and residual anisotropic diffusion in gray matter areas while increasing our signal-to-noise ratio (after averaging), dMRI scans were acquired along 3 orthogonal directions of diffusion. No white matter areas was considered for this study.

Localized magnetic resonance spectra were acquired [localization by adiabatic selective refocusing sequence (46); TE, 25 ms; TR, 3500 ms; 128 averages] from a voxel (2 × 2 × 1.5 mm^3) positioned across both OBs. B_0 shimming was performed using the MAPSHIM Bruker routine leading to typical water line widths of 13 ± 3 Hz. Water suppression was achieved using variable pulse power and optimized relaxation delays (47). The chemical shift displacement artifact was a spatial shift of 18% between water and lipids.

The total duration of each MRI examination was approximately 90 minutes. During this time, animals were anesthetized with 1.5% to 2% isoflurane in pure dioxygen. Their respiration rate was monitored (50-60 breaths/min), and their body temperature was maintained at 37°C ± 0.5°C using a heated water circuit incorporated into the cradle. The head was placed prone and was restrained in a stereotactic manner by a bite bar and ear pins.

Immunohistologic studies

At 8 months after irradiation, mice underwent perfusion with saline solution and, after complete blood removal, with 4% paraformaldehyde. Tissue slices of 20 μm thickness were sectioned using a cryostat (Microm HM 560; Thermo Scientific).

Immunohistochemical staining for Sox-2 (ab97959, 1:200; Abcam), Doublecortin (DCX) (ab18723, 1:100; Abcam), and NeuN (MAB377X, Alexa Fluor 488 conjugated, 1:500; Millipore) was used to characterize neurogenesis by detection of NSCs, immature neurons, and mature neurons, respectively. The revelation was achieved by Alexa Fluor 488−conjugated secondary antibody (ab96919, 1:200; Abcam), and staining was achieved by incubation with 4′,6-diamidino-2-phenylindole dihydrochloride. Brain slices were examined under a fluorescence microscope (Axio Observer Z1 microscope; Carl Zeiss MicroImaging, Jena, Germany) with a 20× objective. Sox-2, DCX, and NeuN immunostainings were quantified by the ratios of the numbers of positive pixels versus 4′,6-diamidino-2-phenylindole dihydrochloride staining.

Data processing

Anatomic MRI

T2-weighted MRI scans were used to measure whole-brain volume by manual segmentation on all acquired slices (from the OBs to upstream of the cerebellum) by using ImageJ software (W. S. Rasband and National Institutes of Health).

Diffusion MRI

Diffusion-sensitized EPI images acquired over 3 independent directions and 3 repetitions were averaged before processing

to improve the signal-to-noise ratio. Diffusion MRI data were processed using homemade software implemented with MATLAB (The MathWorks, Natick, MA). The non-Gaussian diffusion parameters—apparent diffusion coefficient (ADC_0) and kurtosis (K)—were estimated by fitting the signal obtained at all b values according to the intravoxel incoherent motion (IVIM)−non-Gaussian diffusion model (44). The overall measured signal for each region of interest (ROI) can be modeled as follows, assuming signal levels remain high compared with background noise (44):

$$S(b) = S_0\{f_{IVIM}\exp(-bD*) + (1-f_{IVIM})\exp[-bADC_0 + (bADC_0)^2 k/6]\}$$

where S_0 is the signal acquired at $b = 0$, f_{IVIM} is the vascular volume fraction in the tissue, $D*$ is the pseudo-diffusion coefficient associated with the incoherent microcirculation of blood, and ADC_0 is the virtual apparent diffusion coefficient for low b values. K characterizes the deviation from monoexponential decay and is null when water Brownian motion obeys a Gaussian law. As such, K increases with the heterogeneity of the cellular environment. Even though IVIM was accounted for in our model to increase its accuracy, f_{IVIM} and $D*$ parametric maps were not considered for this study.

Brain microstructural alterations were investigated in the cortex, thalamus, striatum, and neurogenic areas (hippocampus, SVZ, and OBs). ROIs were delimited manually over several consecutive slices with objective and similar criteria between animals and study times based on the non−diffusion-weighted EPI images ($b = 0$ s/mm^2): cortex (7 slices), hippocampus (2 slices), thalamus (3 slices), striatum (2 slices), SVZ (2 slices), and OBs (3 slices).

Moreover, a new diffusion composite metric, designated the S-index (an abbreviation for signature index), was evaluated in this study. The general basic concept for the S-index (45) is to directly compare (using a simple distance calculation) the dMRI signals of the tissue under investigation with those of a library of typical signals, without using any diffusion model to obtain direct tissue pattern recognition. Furthermore, to increase sensitivity, only signals acquired at "key" b values (diffusion weighting) known to be the most sensitive to changes in tissue structure are used. In this study, a library of 2 generic dMRI signals—one representing normal mouse brain tissue and the other mimicking the same tissue undergoing a moderate degree of cell proliferation—was built in advance. The S-index corresponds to the proximity of the signal of the tissue under investigation with those 2 signals, in such a way that 45 corresponds to the generic normal tissue and 75 to the generic proliferating tissue. An index >75 means that the tissue is undergoing more structural changes than the generic proliferating tissue, while an S-index between 45 and 75 corresponds to a milder change in tissue structure. For this study, the 2 key b values considered were $b = 200$ s/mm^2 and $b = 1500$ s/mm^2. The library of diffusion signals for both b values was built using the IVIM−diffusion kurtosis model (44) with the following parameters corresponding to each reference tissue: $ADC_0 = 0.75\ 10^{-4}$ mm^2/s, $K = 0.6$, $f_{IVIM} = 1\%$, and $D* = 0.01$ mm^2/s for generic young neural tissue and $ADC_0 = 0.65\ 10^{-4}$ mm^2/s, $K = 0.8$, $f_{IVIM} = 3\%$, and $D* = 0.03$ mm^2/s for neural tissue undergoing moderate cell growth.

Magnetic resonance spectroscopy

Spectra were analyzed using LCModel (48) and a simulated basis set. Twenty metabolites were considered, and the macromolecule baseline was parameterized as described elsewhere (49). Metabolite concentrations were derived using total creatine (ie, 8 mmol/L) as an internal reference of concentration.

Statistical analyses

All data are presented as means ± standard deviations. The statistical analyses were performed with StatView SE software

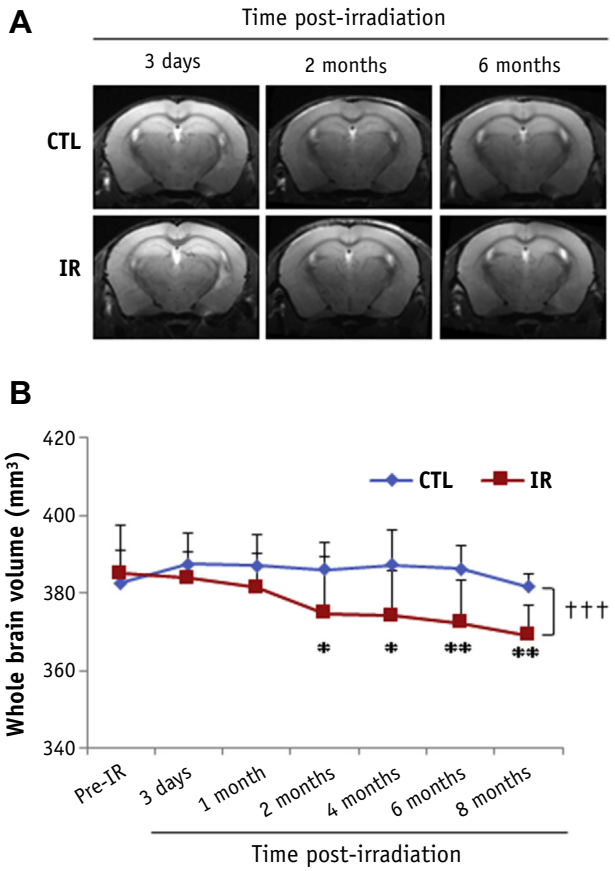

Fig. 1. Whole-brain radiotherapy induces significant long-lasting cerebral atrophy. A, Representative T2-weighted magnetic resonance imaging scans obtained from control (CTL) and irradiated (IR) animals at 3 days, 2 months, and 6 months after brain irradiation (3 fractions of 5 Gy). B, Average whole-brain volume before irradiation (Pre-IR) and at different times after irradiation for IR and CTL mice. Data are presented as mean ± standard deviation, with n = 15 for both groups. One asterisk indicates $P < .05$ versus CTL group (Student t test); 2 asterisks, $P < .01$ versus CTL group (Student t test); and 3 daggers, $P < .0001$ for comparison between CTL and IR curves (Bonferroni post hoc test after significant 2-way analysis of variance [group and time effects]).

(SAS Institute). For comparisons between groups (control and irradiated mice) at any time after irradiation, significance levels were assessed using the Student *t* test. The statistical significance between time courses (all times combined) for irradiated or control animals was obtained by 2-way analysis of variance (group and time effects) corrected for multiple comparisons using Bonferroni post hoc. To evaluate correlations between 2 parameters, the Pearson correlation coefficient (*R*) and *z* test (*P* value) were determined.

Results

Mouse brain atrophy induced by high-dose irradiation

T2-weighted MRI scans did not show any noticeable anatomic lesions, such as edema or necrosis, at any time after brain irradiation (Fig. 1A). However, whole-brain volume assessment from anatomic MRI revealed significant long-lasting irradiation-induced brain atrophy of 5% (Fig. 1B, $P < 10^{-4}$).

Diffusion parameters (ADC_0 and kurtosis) highlight irradiation-induced injury in OBs but not in other brain regions

We first selected 3 readily identifiable brain structures to study irradiation-induced damage: the cortex, the thalamus, and the striatum. Both diffusion parameters (ADC_0 and kurtosis) evolved similarly in the cortex (Fig. E1, available online at https://doi.org/10.1016/j.ijrobp.2018.01.070), thalamus (Fig. E2, available online at https://doi.org/10.1016/j.ijrobp.2018.01.070), and striatum (Fig. E3, available online at https://doi.org/10.1016/j.ijrobp.2018.01.070) of controls and irradiated mice. These results show that high-dose irradiation did not significantly alter the microstructural organization in these nonneurogenic areas.

We have previously reported that irradiation with 3 fractions of 5 Gy induced a long-term decrease in the number of NSCs and progenitors in neurogenic areas without inducing chronic neuroinflammation (15, 17). Thus, we tested whether dMRI could detect irradiation-induced alterations in the SVZ and hippocampus. Because of the small size of the SVZ in the adult mouse (50), special care was given to its delimitation. As illustrated in

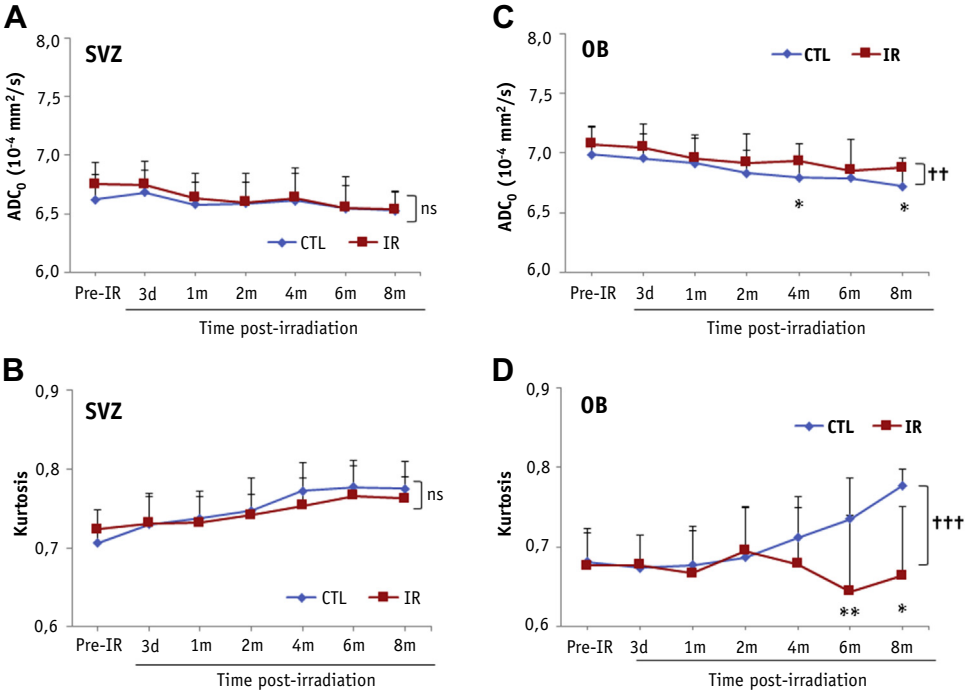

Fig. 2. Quantitative diffusion magnetic resonance imaging detects irradiation-induced injury in the olfactory bulbs (OBs) but not in the subventricular zone (SVZ). Time courses of values of non-Gaussian parameters, apparent diffusion coefficient (ADC_0) (A) and kurtosis (B), in SVZ and quantification of non-Gaussian parameters, ADC_0 (C) and kurtosis (D), in OBs at different times after whole-brain irradiation. Data are presented as mean ± standard deviation, with 15 nonirradiated mice (control [CTL] group) and 15 irradiated (IR) mice. One asterisk indicates $P < .05$ versus CTL group (Student *t* test); 2 asterisks, $P < .01$ versus CTL group (Student *t* test); 2 daggers, $P < .01$ for comparison between CTL and IR curves (Bonferroni post hoc test after significant 2-way analysis of variance [group and time effects]); and 3 daggers, $P < .0001$ for comparison between CTL and IR curves (Bonferroni post hoc test after significant 2-way analysis of variance [group and time effects]). ns = nonsignificant difference; Pre-IR = before irradiation.

Figure E4A (available online at https://doi.org/10.1016/j.ijrobp.2018.01.070), consistent and robust ROI sizes were achieved in irradiated and control animals. Noticeably, ADC_0 ($P < 10^{-4}$) and kurtosis ($P < 10^{-4}$) values were significantly different between the SVZ and the striatum, the adjacent brain structure, highlighting microstructural differences between these regions (Figs. E4B and E4C, available online at https://doi.org/10.1016/j.ijrobp.2018.01.070).

For the hippocampus, our dMRI data analysis showed a transient increase in ADC_0 3 days after irradiation (Fig. E5C, available online at https://doi.org/10.1016/j.ijrobp.2018.01.070; $P < .01$) but no changes in kurtosis (Fig. E5D, available online at https://doi.org/10.1016/j.ijrobp.2018.01.070). Concerning the SVZ, no significant changes were observed between control and irradiated mice, although higher kurtosis values were found in irradiated animals for >2 months after treatment (Figs. 2A and 2B).

As irradiation of the SVZ with 3 fractions of 5 Gy has been shown to induce a long-term decrease in the number of newborn neurons reaching the OBs (15), we next investigated the dMRI signals in this brain structure. As illustrated in Figure 2C, ADC_0 values were greater in the OBs of irradiated mice ($P < .05$ at 4 and 8 months). In parallel, a large reduction in kurtosis was observed 4 months after irradiation and maintained until the end of the study ($P < 10^{-4}$, Fig. 2D).

Diffusion S-index reveals microstructural changes in neurogenic areas and OBs of irradiated animals

By use of the S-index approach (45), no significant irradiation effect was detected in the nonneurogenic areas (cortex, thalamus, and striatum), as shown in Figures E1B, E2B, and E3B (available online at https://doi.org/10.1016/j.ijrobp.2018.01.070). Only a transient decrease in the S-index was observed in the hippocampus of irradiated animals as compared with the control group on day 3 after irradiation (Fig. E5B, available online at https://doi.org/10.1016/j.ijrobp.2018.01.070; $P < .05$). These results are supported by the MRS data obtained in the hippocampus. The metabolite concentrations in the hippocampus were relatively similar between the groups, apart from a decrease in neuronal metabolites N-acetylaspartate and gamma-aminobutyric acid (GABA) only at 1 month after irradiation

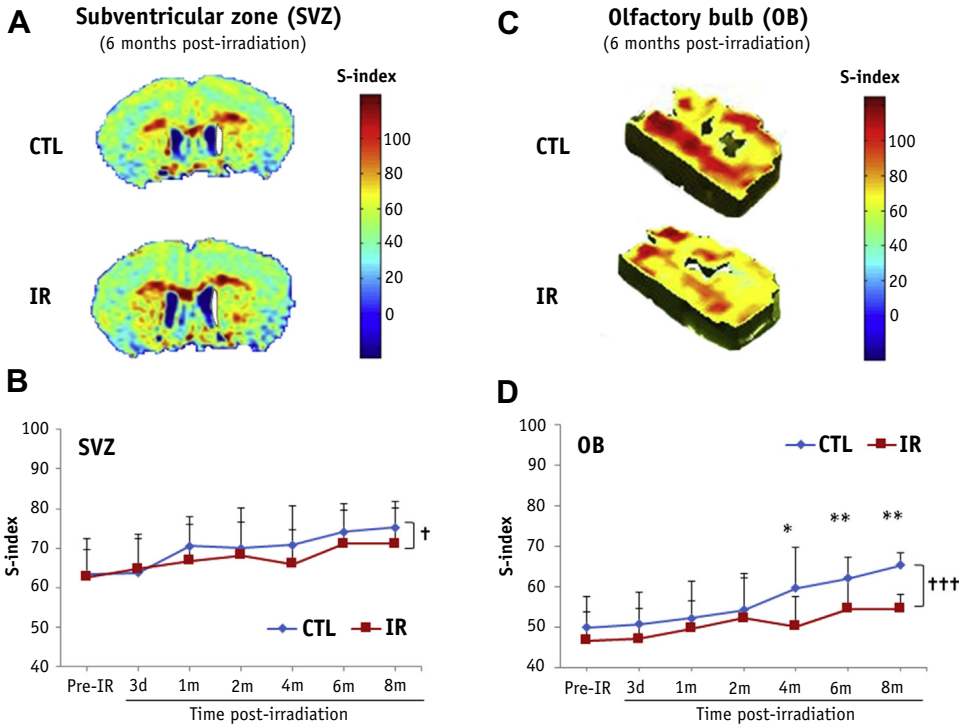

Fig. 3. The diffusion S-index is more sensitive to damage induced by irradiation in the subventricular zone (SVZ) and the olfactory bulbs (OBs) than non-Gaussian diffusion parameters. A, S-index maps including SVZ from control (CTL) and irradiated (IR) mice 6 months after irradiation. B, Quantification of S-index in SVZ at different times after irradiation. C, Three-dimensional rendering of our S-index maps in the OBs for 2 CTL and IR mice 6 months after irradiation. D, Time courses of average S-index in OBs before and up to 8 months after whole-brain irradiation. Data are presented as mean ± standard deviation, with 15 nonirradiated mice (CTL group) and 15 IR mice. One asterisk indicates $P < .05$ versus CTL group (Student *t* test); 2 asterisks, $P < .01$ versus CTL group (Student *t* test); 1 dagger, $P < .05$ for comparison between CTL and IR curves (Bonferroni post hoc test after significant 2-way analysis of variance [group and time effects]); and 3 daggers, $P < .0001$ for comparison between CTL and IR curves (Bonferroni post hoc test after significant 2-way analysis of variance [group and time effects]). Pre-IR = before irradiation.

(Figs. E6A and E6B, available online at https://doi.org/10.1016/j.ijrobp.2018.01.070). These changes could reflect a temporary neuronal (apparently GABAergic) deficit. It is tempting to link those metabolic changes to the earlier (at 3 days after cranial irradiation) and similarly transient decrease in the S-index observed in the same right hippocampus (Fig. E5, available online at https://doi.org/10.1016/j.ijrobp.2018.01.070).

An interesting finding was that the longitudinal follow-up of animals highlighted a persistent decrease in S-index values in the irradiated mice compared with controls from 1 month to 8 months after brain irradiation (Figs. 3A and 3B, $P < .05$). Moreover, the 3-dimensional S-index maps revealed important microstructural changes in the OBs after brain irradiation (Fig. 3C). Indeed, a significant S-index drop was noticed in irradiated mice compared with control animals (Fig. 3D, $P < 10^{-4}$). This S-index decrease was observed from 4 months after irradiation, and this effect was maintained until the end of the study and therefore mirrored the increase in ADC_0 and the reduction in kurtosis (Figs. 2C and 2D, respectively).

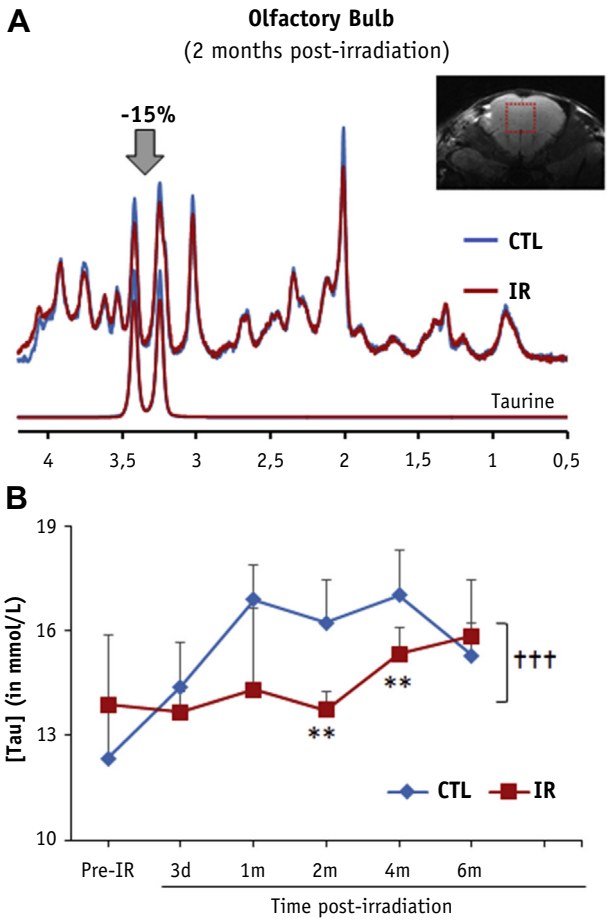

Fig. 4. Taurine levels are decreased in the olfactory bulbs after whole-brain irradiation. A, ^{1}H magnetic resonance spectra and corresponding taurine contributions from control (CTL) and irradiated (IR) mice (spectra averaged from all animals for each group) obtained at 2 months after irradiation. B, Time courses of taurine concentrations in olfactory bulbs for both CTL and IR groups. Data are presented as mean ± standard deviation, with 15 nonirradiated mice (CTL group) and 15 IR mice. Two asterisks indicate $P < .01$ versus CTL group (Student t test); and 3 daggers, $P < .0001$ for comparison between CTL and IR curves (Bonferroni post hoc test after significant 2-way analysis of variance [group and time effects]). Pre-IR = before irradiation.

To further explore the irradiation-induced alterations in the OBs, we conducted a longitudinal follow-up of brain metabolite concentrations using localized MRS (from a 6-μL voxel encompassing both OBs). As presented in Figure 4A, ^{1}H spectra exhibited significantly lowered levels of taurine in irradiated mice compared with those in the control group (Fig. 4B, $P < 10^{-4}$). This decrease was accompanied by similarly reduced levels of GABA (Fig. E7, available online at https://doi.org/10.1016/j.ijrobp.2018.01.070).

Finally, to confirm the long-term effects of irradiation on the SVZ and OBs at the histologic level, we performed immunohistologic studies using antibodies directed against Sox-2, a marker of neural progenitors; DCX, a marker of immature neurons; and NeuN, a marker of mature neurons, at the end of the experiment (ie, 8 months after irradiation). We found a significant decrease in Sox-2−positive cells in the SVZ ($P < .05$) (Figs. 5A and 5C) and a major decline in DCX in the OBs ($P < .0001$) (Figs. 5B and 5C) of irradiated animals, in accordance with previous reports showing a decreased number of proliferating neural progenitors in the irradiated SVZ and its direct consequence, the decreased arrival of newborn neurons in the OBs (15, 17). In parallel, a decrease in NeuN-positive cells was observed in the OBs of irradiated mice compared with control mice ($P < .05$, Figs. 5B and 5C). Correlations between S-index values and immunostaining against progenitors and immature neurons in the SVZ and OBs reflect the sensitivity of the S-index for irradiation-induced injury in the neurogenic areas, especially the correlation between the S-index and DCX immunostaining performed in the OBs at the end of the experiment ($R^2 = 0.39$, $P = .09$; Fig. E8, available online at https://doi.org/10.1016/j.ijrobp.2018.01.070). These histologic data are consistent with our MRS and MRI findings evidencing the metabolic and structural alterations progressively induced in the SVZ and/or OBs of irradiated animals.

Discussion

Neurocognitive disorders are a frequent long-term effect of brain RT. Development of specific noninvasive biomarkers is still required for diagnosing and monitoring disease progression. In this longitudinal study, we show that a new composite dMRI biomarker, the S-index, is more sensitive than the conventional diffusion parameters, ADC_0 and kurtosis, as demonstrated by its greater statistical significance, revealing tissue microstructure changes associated

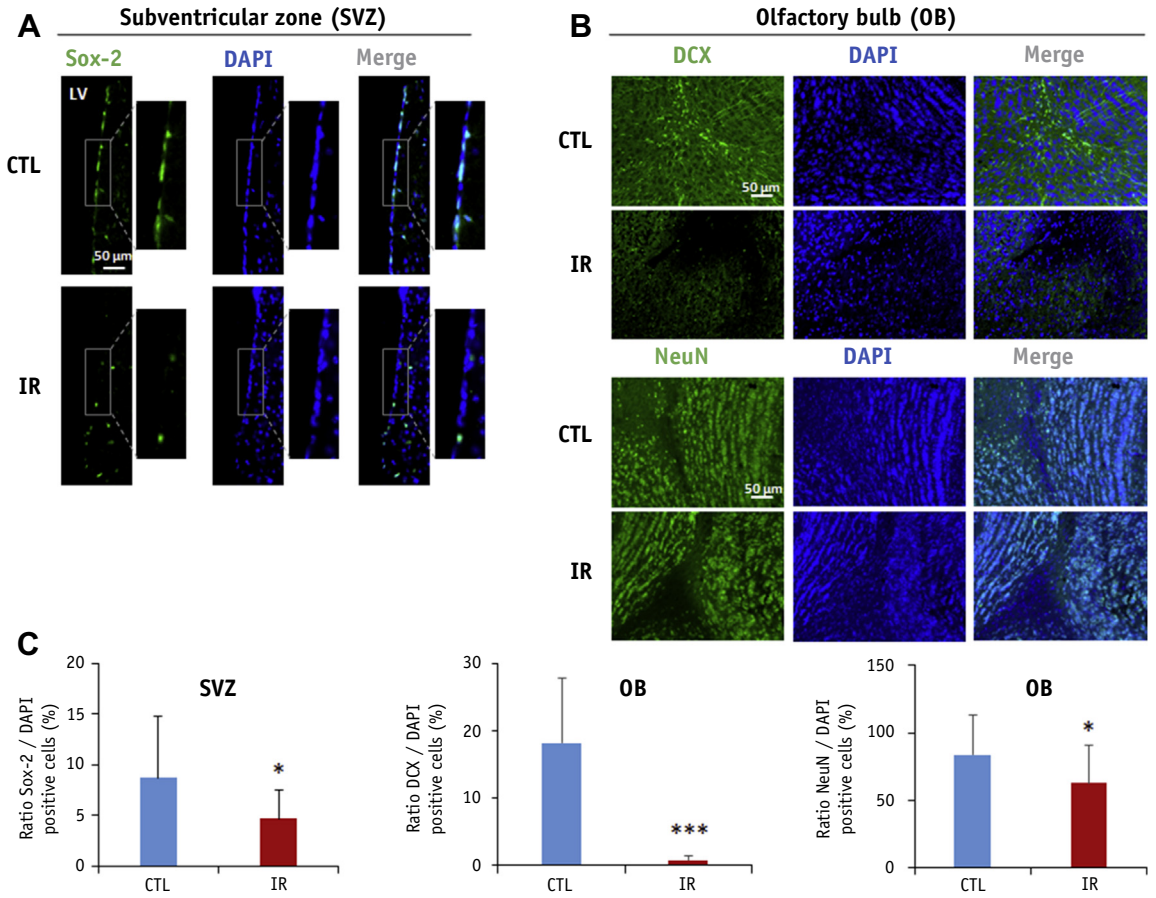

Fig. 5. Whole-brain irradiation impairs neurogenesis, affecting neural stem cells in the subventricular zone (SVZ) and neuronal migration into the olfactory bulbs (OBs). A and B, Representative Sox-2 (specific marker for neural stem cells), Doublecortin (DCX) (specific marker for immature neurons), NeuN (specific marker for mature neurons), and 4′,6-diamidino-2-phenylindole dihydrochloride (DAPI) (DNA intercalator to identify cell nuclei) immunofluorescence in SVZ (A) or OBs (B) of irradiated (IR) or control (CTL) animals at 8 months after cranial irradiation. The scale bar is equivalent to 50 µm. LV = lateral ventricle. C, Quantification of Sox-2−positive cells in SVZ and DCX or NeuN-positive cells in OBs. Data are presented as mean ± standard deviation, with 5 nonirradiated mice (CTL group) and 3 IR mice with at least 3 photographs per animal (for each type of immunostaining and each studied area). One asterisk indicates $P < .05$ versus CTL group (Student t test); and 3 asterisks, $P < .0001$ versus CTL group (Student t test).

with neurogenesis decline in the irradiated mouse SVZ and OBs. In parallel, decreased levels of taurine are observed in the OBs from 2 months after irradiation and maintained until the end of the experiment.

In our preclinical model of RT, only late irradiation-induced damage in the OBs after whole-brain irradiation resulted in changes in individual dMRI parameters. Roughly, ADC_0 reflects the mobility of water in tissues, mainly in extracellular space, and is influenced by its viscosity and its tortuosity (cell filling depending on the density, shape, and size of the brain cells). Kurtosis characterizes the deviation of this Brownian motion from a Gaussian (free) diffusion pattern, reflecting hindrance or restriction of diffusion-driven water molecular displacements by obstacles, such as cell membranes or fibers. The observation of increased ADC_0 values along with a diminution of kurtosis values from 4 months until 8 months after irradiation suggests a decreasing cell density in the OBs. In the same way, Gazdzinski et al (51) and de Guzman et al (52) have evidenced notable effects in the OBs after fetal irradiation that displayed both a detectable volume deficit and a loss in neurogenesis for most doses and for age. Although these data were obtained after irradiation at different developmental stages, they are consistent with the irradiation-induced effects on the OBs we have highlighted with dMRI in this study. Is it interesting that we also found an important decrease in taurine and GABA concentrations in the OBs from 2 months after whole-brain irradiation. Both taurine (42, 53, 54) and GABA (55, 56) have been shown to promote neurogenesis. Their specific decrease in the OBs is thus consistent with the irradiation-induced decrease in bulbar neurogenesis.

One of the major obstacles of dMRI in analyzing neurogenic areas in mice is the small size of these regions

in mice. We ensured the robustness of our delimitation of the SVZ by checking (*1*) that the number of the ROI pixels was similar between the animals and over time and (*2*) that the ADC_0 and kurtosis values were significantly different between the SVZ and the striatum, the neighboring brain structure.

The neurogenesis decline induced by high-dose irradiation has been abundantly documented (15, 17, 57, 58). Lazarini et al (15) have shown that the focal irradiation of the SVZ, using the same doses of irradiation (3 fractions of 5 Gy) used in our study protocol, dramatically decreased the rate of production of new OB neurons for up to 7 months after irradiation exposure with long-term olfactory memory affected. In accordance with these studies, we have observed a decrease in Sox-2−positive NSCs in the SVZ and in DCX-positive newborn neurons in the OBs in irradiated animals, reflecting the perturbations of proliferation of NSCs in the SVZ as well as the reduced migration of newborn cells to the OBs (59). Consistently with this neurogenesis decline, we found a decrease in S-index values in the irradiated SVZ from 1 month until the end of the experiment (8 months after irradiation). This longitudinal follow-up with dMRI, initiated for the first time in a mouse model, allowed us to highlight different kinetics in the irradiation-induced alterations between the SVZ and the OBs, consistent with the alteration of OBs as a consequence of SVZ neurogenesis decline.

Overall, our data show that the S-index, which is optimized to take into account both Gaussian and non-Gaussian diffusion, is a more sensitive biomarker of neurogenesis alteration, allowing the detection of irradiation-induced microstructure alterations in the SVZ, and could thus represent an interesting approach for the monitoring of neurogenesis in discrete areas of the human brain. The other main neurogenic area in the adult mouse brain, the SGZ of the dentate gyrus in the hippocampus, has an even smaller volume than the SVZ. For practical reasons, we opted to delimit a larger ROI encompassing the whole dorsal hippocampus. The irradiation-induced perturbation of SGZ neurogenesis has been reported not to occur before several months after cranial irradiation (17, 20, 42, 43, 60), but neither ADC_0, kurtosis, nor the S-index revealed any significant microstructural alterations in this larger ROI. As the size of our "hippocampal" ROI and the subsequent partial volume effect are likely reasons to explain our inability to detect those expected irradiation-induced alterations in the SGZ, future dMRI studies should work on improving the anatomic specificity of this ROI. Even though both ADC_0 and the S-index revealed transient hippocampus alterations 3 days after irradiation, further studies are needed to determine whether they are related to the monocyte infiltration known to occur in the days that follow the irradiation.

Studying neurogenic areas using MRI remains a great challenge (21, 61, 62) that requires the acquisition of data at high spatial resolution. Diffusion MRI and especially the S-index appear particularly well adapted. Indeed, our data demonstrate that the S-index approach is more sensitive than standard dMRI parameters, ADC_0 and kurtosis, considered separately. In the context of this study, that is, brain injury induced by irradiation, this new methodologic approach has permitted a decrease in cell density (reflected by lower S-index values) in 2 areas of interest to be exhibited, which is in accordance with the well-known effects of high-dose irradiation on neurogenic niches.

The SVZ in the adult human brain is less active than in rodents. However, this neurogenic area could be restimulated to produce neurons or oligodendrocytes in various pathologies such as neurodegenerative or psychiatric diseases (63, 64), with the SVZ being stimulated in stroke, epilepsy, Huntington disease, or multiple sclerosis (65, 66). We have shown that even with placement under excellent experimental conditions, conventional dMRI would have a hard time monitoring irradiation-induced alterations in the mouse SGZ. However, our results clearly show that the S-index has the potential to detect low cell density changes even in a small structure such as the mouse SVZ.

Conclusions

The overall results of this preclinical study suggest that diffusion-weighted MRI, especially through the S-index, is a relevant imaging biomarker to monitor brain irradiation injury noninvasively and probe structural changes underlying the irradiation-induced cognitive deficits, in particular the neurogenesis decline supposed to be one of the major causes of irradiation-induced cognitive impairment. Future studies will further investigate the clinical potential of the S-index dMRI approach, especially for the monitoring (diagnosis and therapy assessment) of various pathologies associated with tissue microstructure alterations, such as irradiation-induced lesions.

References

1. Chang EL, Wefel JS, Hess KR, et al. Neurocognition in patients with brain metastases treated with radiosurgery or radiosurgery plus whole-brain irradiation: A randomised controlled trial. *Lancet Oncol* 2009;10:1037-1044.
2. Bodensohn R, Corradini S, Ganswindt U, et al. A prospective study on neurocognitive effects after primary radiotherapy in high-grade glioma patients. *Int J Clin Oncol* 2016;21:642-650.
3. Brown PD, Jaeckle K, Ballman KV, et al. Effect of radiosurgery alone vs radiosurgery with whole brain radiation therapy on cognitive function in patients with 1 to 3 brain metastases: A randomized clinical trial. *JAMA* 2016;316:401-409.
4. Roman DD, Sperduto PW. Neuropsychological effects of cranial radiation: Current knowledge and future directions. *Int J Radiat Oncol Biol Phys* 1995;31:983-998.
5. Yuksek E, Eroz S, Yassa A, et al. The influences of whole brain radiotherapy on social cognition and association with hippocampal and frontal dosimetry. *Psychiatr Q* 2015;86:533-543.
6. Agbahiwe H, Rashid A, Horska A, et al. A prospective study of cerebral, frontal lobe, and temporal lobe volumes and

neuropsychological performance in children with primary brain tumors treated with cranial radiation. *Cancer* 2017;123:161-168.
7. Tofilon PJ, Fike JR. The radioresponse of the central nervous system: A dynamic process. *Radiat Res* 2000;153:357-370.
8. Belka C, Budach W, Kortmann RD, et al. Radiation induced CNS toxicity—Molecular and cellular mechanisms. *Br J Cancer* 2001;85:1233-1239.
9. Kim JH, Brown SL, Jenrow KA, et al. Mechanisms of radiation-induced brain toxicity and implications for future clinical trials. *J Neurooncol* 2008;87:279-286.
10. Greene-Schloesser D, Robbins ME. Radiation-induced cognitive impairment—From bench to bedside. *Neuro Oncol* 2012;14(Suppl. 4):iv37-iv44.
11. Greene-Schloesser D, Robbins ME, Peiffer AM, et al. Radiation-induced brain injury: A review. *Front Oncol* 2012;2:73.
12. Wilke C, Grosshans D, Duman J, et al. Radiation-induced cognitive toxicity: Pathophysiology and interventions to reduce toxicity in adults. *Neuro Oncol* 2018;20:597-607.
13. Zhao W, Robbins ME. Inflammation and chronic oxidative stress in radiation-induced late normal tissue injury: Therapeutic implications. *Curr Med Chem* 2009;16:130-143.
14. Furuse M, Nonoguchi N, Kawabata S, et al. Delayed brain radiation necrosis: Pathological review and new molecular targets for treatment. *Med Mol Morphol* 2015;48:183-190.
15. Lazarini F, Mouthon MA, Gheusi G, et al. Cellular and behavioral effects of cranial irradiation of the subventricular zone in adult mice. *PLoS One* 2009;4:e7017.
16. Monje M, Dietrich J. Cognitive side effects of cancer therapy demonstrate a functional role for adult neurogenesis. *Behav Brain Res* 2012;227:376-379.
17. Pineda JR, Daynac M, Chicheportiche A, et al. Vascular-derived TGF-β increases in the stem cell niche and perturbs neurogenesis during aging and following irradiation in the adult mouse brain. *EMBO Mol Med* 2013;5:548-562.
18. Farjam R, Pramanik P, Aryal MP, et al. A radiation-induced hippocampal vascular injury surrogate marker predicts late neurocognitive dysfunction. *Int J Radiat Oncol Biol Phys* 2015;93:908-915.
19. Yoritsune E, Furuse M, Kuwabara H, et al. Inflammation as well as angiogenesis may participate in the pathophysiology of brain radiation necrosis. *J Radiat Res* 2014;55:803-811.
20. Son Y, Yang M, Wang H, et al. Hippocampal dysfunctions caused by cranial irradiation: A review of the experimental evidence. *Brain Behav Immun* 2015;45:287-296.
21. Yang L, Yang J, Li G, et al. Pathophysiological responses in rat and mouse models of radiation-induced brain injury. *Mol Neurobiol* 2017;54:1022-1032.
22. Ming G-L, Song H. Adult neurogenesis in the mammalian brain: Significant answers and significant questions. *Neuron* 2011;70:687-702.
23. Eichenbaum H, Dudchenko P, Wood E, et al. The hippocampus, memory, and place cells: Is it spatial memory or a memory space? *Neuron* 1999;23:209-226.
24. Rola R, Raber J, Rizk A, et al. Radiation-induced impairment of hippocampal neurogenesis is associated with cognitive deficits in young mice. *Exp Neurol* 2004;188:316-330.
25. Raber J, Rola R, LeFevour A, et al. Radiation-induced cognitive impairments are associated with changes in indicators of hippocampal neurogenesis. *Radiat Res* 2004;162:39-47.
26. Amano T, Inamura T, Wu CM, et al. Effects of single low dose irradiation on subventricular zone cells in juvenile rat brain. *Neurol Res* 2002;24:809-816.
27. Le Bihan D, Iima M. Diffusion magnetic resonance imaging: What water tells us about biological tissues. *PLoS Biol* 2015;13:e1002203.
28. Nagesh V, Tsien CI, Chenevert TL, et al. Radiation-induced changes in normal-appearing white matter in patients with cerebral tumors: A diffusion tensor imaging study. *Int J Radiat Oncol Biol Phys* 2008;70:1002-1010.
29. Hope TR, Vardal J, Bjørnerud A, et al. Serial diffusion tensor imaging for early detection of radiation-induced injuries to normal-appearing white matter in high-grade glioma patients. *J Magn Reson Imaging* 2015;41:414-423.
30. Zhu H, Barker PB. MR spectroscopy and spectroscopic imaging of the brain. *Methods Mol Biol* 2011;711:203-226.
31. Zeng Q-S, Li C-F, Liu H, et al. Distinction between recurrent glioma and radiation injury using magnetic resonance spectroscopy in combination with diffusion-weighted imaging. *Int J Radiat Oncol Biol Phys* 2007;68:151-158.
32. Elias AE, Carlos RC, Smith EA, et al. MR spectroscopy using normalized and non-normalized metabolite ratios for differentiating recurrent brain tumor from radiation injury. *Acad Radiol* 2011;18:1101-1108.
33. Lee MC, Pirzkall A, McKnight TR, et al. 1H-MRSI of radiation effects in normal-appearing white matter: Dose-dependence and impact on automated spectral classification. *J Magn Reson Imaging* 2004;19:379-388.
34. Sundgren PC, Nagesh V, Elias A, et al. Metabolic alterations: A biomarker for radiation-induced normal brain injury—An MR spectroscopy study. *J Magn Reson Imaging* 2009;29:291-297.
35. Peiffer AM, Shi L, Olson J, et al. Differential effects of radiation and age on diffusion tensor imaging in rats. *Brain Res* 2010;1351:23-31.
36. Trivedi R, Khan AR, Rana P, et al. Radiation-induced early changes in the brain and behavior: Serial diffusion tensor imaging and behavioral evaluation after graded doses of radiation. *J Neurosci Res* 2012;90:2009-2019.
37. Wang S, Tryggestad E, Zhou T, et al. Assessment of MRI parameters as imaging biomarkers for radiation necrosis in the rat brain. *Int J Radiat Oncol Biol Phys* 2012;83:e431-e436.
38. Kumar M, Haridas S, Trivedi R, et al. Early cognitive changes due to whole body γ-irradiation: A behavioral and diffusion tensor imaging study in mice. *Exp Neurol* 2013;248:360-368.
39. Gupta M, Mishra SK, Kumar BSH, et al. Early detection of whole body radiation induced microstructural and neuroinflammatory changes in hippocampus: A diffusion tensor imaging and gene expression study. *J Neurosci Res* 2017;95:1067-1078.
40. Herynek V, Burian M, Jirák D, et al. Metabolite and diffusion changes in the rat brain after Leksell Gamma Knife irradiation. *Magn Reson Med* 2004;52:397-402.
41. Xu S, Zhuo J, Racz J, et al. Early microstructural and metabolic changes following controlled cortical impact injury in rat: A magnetic resonance imaging and spectroscopy study. *J Neurotrauma* 2011;28:2091-2102.
42. Rana P, Khan AR, Modi S, et al. Altered brain metabolism after whole body irradiation in mice: A preliminary in vivo 1H MRS study. *Int J Radiat Biol* 2013;89:212-218.
43. Gupta M, Rana P, Trivedi R, et al. Comparative evaluation of brain neurometabolites and DTI indices following whole body and cranial irradiation: A magnetic resonance imaging and spectroscopy study. *NMR Biomed* 2013;26:1733-1741.
44. Iima M, Yano K, Kataoka M, et al. Quantitative non-Gaussian diffusion and intravoxel incoherent motion magnetic resonance imaging: Differentiation of malignant and benign breast lesions. *Invest Radiol* 2015;50:205-211.
45. Iima M, Le Bihan D. Clinical intravoxel incoherent motion and diffusion MR imaging: Past, present, and future. *Radiology* 2016;278:13-32.
46. Garwood M, DelaBarre L. The return of the frequency sweep: Designing adiabatic pulses for contemporary NMR. *J Magn Reson* 2001;153:155-177.
47. Tkác I, Starcuk Z, Choi IY, et al. In vivo 1H NMR spectroscopy of rat brain at 1 ms echo time. *Magn Reson Med* 1999;41:649-656.

48. Provencher SW. Estimation of metabolite concentrations from localized in vivo proton NMR spectra. *Magn Reson Med* 1993;30:672-679.
49. Lopez-Kolkovsky AL, Mériaux S, Boumezbeur F. Metabolite and macromolecule T1 and T2 relaxation times in the rat brain in vivo at 17.2T. *Magn Reson Med* 2016;75:503-514.
50. Merkle FT, Fuentealba LC, Sanders TA, et al. Adult neural stem cells in distinct microdomains generate previously unknown interneuron types. *Nat Neurosci* 2014;17:207-214.
51. Gazdzinski LM, Cormier K, Lu FG, et al. Radiation-induced alterations in mouse brain development characterized by magnetic resonance imaging. *Int J Radiat Oncol Biol Phys* 2012;84:e631-e638.
52. de Guzman AE, Gazdzinski LM, Alsop RJ, et al. Treatment age, dose and sex determine neuroanatomical outcome in irradiated juvenile mice. *Radiat Res* 2015;183:541-549.
53. Hernández-Benítez R, Ramos-Mandujano G, Pasantes-Morales H. Taurine stimulates proliferation and promotes neurogenesis of mouse adult cultured neural stem/progenitor cells. *Stem Cell Res* 2012;9:24-34.
54. Ripps H, Shen W. Review: Taurine: A "very essential" amino acid. *Mol Vis* 2012;18:2673-2686.
55. Miranda-Contreras L, Ramirez-Martens LM, Benitez-Diaz PR, et al. Levels of amino acid neurotransmitters during mouse olfactory bulb neurogenesis and in histotypic olfactory bulb cultures. *Int J Dev Neurosci* 2000;18:83-91.
56. Pallotto M, Deprez F. Regulation of adult neurogenesis by GABAergic transmission: Signaling beyond GABAA-receptors. *Front Cell Neurosci* 2014;8:166.
57. Achanta P, Capilla-Gonzalez V, Purger D, et al. Subventricular zone localized irradiation affects the generation of proliferating neural precursor cells and the migration of neuroblasts. *Stem Cells* 2012;30:2548-2560.
58. Balentova S, Hajtmanova E, Trylcova R, et al. Ionizing radiation induced long-term alterations in the adult rat rostral migratory stream. *Acta Histochem* 2014;116:265-271.
59. Sakamoto M, Kageyama R, Imayoshi I. The functional significance of newly born neurons integrated into olfactory bulb circuits. *Front Neurosci* 2014;8:121.
60. Andres-Mach M, Rola R, Fike JR. Radiation effects on neural precursor cells in the dentate gyrus. *Cell Tissue Res* 2008;331:251-262.
61. Manganas LN, Zhang X, Li Y, et al. Magnetic resonance spectroscopy identifies neural progenitor cells in the live human brain. *Science* 2007;318:980-985.
62. Couillard-Despres S, Aigner L. In vivo imaging of adult neurogenesis. *Eur J Neurosci* 2011;33:1037-1044.
63. Apple DM, Fonseca RS, Kokovay E. The role of adult neurogenesis in psychiatric and cognitive disorders. *Brain Res* 2017;1655:270-276.
64. Winner B, Winkler J. Adult neurogenesis in neurodegenerative diseases. *Cold Spring Harb Perspect Biol* 2015;7:a021287.
65. Curtis MA, Faull RLM, Eriksson PS. The effect of neurodegenerative diseases on the subventricular zone. *Nat Rev Neurosci* 2007;8:712-723.
66. Nait-Oumesmar B, Picard-Riéra N, Kerninon C, et al. The role of SVZ-derived neural precursors in demyelinating diseases: From animal models to multiple sclerosis. *J Neurol Sci* 2008;265:26-31.